PERGAMON

Journal of the Mechanics and Physics of Solids
50 (2002) 1011–1027

JOURNAL OF THE
MECHANICS AND
PHYSICS OF SOLIDS

www.elsevier.com/locate/jmps

# Inhomogeneous deformation in metallic glasses

R. Huang[a,b,*], Z. Suo[b,c], J.H. Prevost[a,b], W.D. Nix[d]

[a] *Department of Civil and Environmental Engineering, Princeton University, Princeton, NJ 08544, USA*
[b] *Princeton Materials Institute, Princeton University, Princeton, NJ 08544, USA*
[c] *Department of Mechanical and Aerospace Engineering, Princeton University, Princeton, NJ 08544, USA*
[d] *Department of Materials Science and Engineering, Stanford University, Stanford, CA 94305, USA*

Received 25 May 2001; accepted 29 August 2001

**Abstract**

The present study provides a theoretical framework for the inhomogeneous deformation in metallic glasses. The free volume concentration is adopted as the order parameter, which is a function of position and time. The three processes that can change the local free volume concentration are diffusion, annihilation, and stress-driven creation. The rate functions for free volume generation and plastic flow depend on the underlying microscopic model, but the framework is generally valid for different models. A simple shear problem is solved as an example. A linear stability analysis is performed on the basis of the homogeneous solution. An inhomogeneous solution is obtained with a finite amplitude disturbance to the initial free volume distribution. Numerical simulation shows the development of the inhomogeneous deformation and strain localization. 

*Keywords:* Metallic glasses; Free volume; Inhomogeneous deformation; Localization

## 1. Introduction

Metallic glasses, also known as amorphous metals, differ from ordinary metals in that their atoms do not assemble on a crystalline lattice. Since the first amorphous metal was formed from the liquid state of an Au–Si alloy by the fast quenching technique (Klement et al., 1960), a great number of amorphous metals have been produced during the last three decades. Prior to the development of bulk metallic glasses, very high cooling rates ($>10^5$ K/s) were required to prevent crystallization and studies of metallic glasses were confined to very thin ribbons or wires (Pampillo, 1975). The

* Corresponding author. Department of Civil and Environmental Engineering, Princeton University, Princeton, NJ 08544, USA. Tel.: +1-609-258-1619; fax: +1-609-258-1270.
*E-mail address:* ruihuang@princeton.edu (R. Huang).

0022-5096/02/$ - see front matter 
PII: S0022-5096(01)00115-6

recent development of bulk metallic glasses (Johnson, 1999) has allowed mechanical testing under a much wider range of loading conditions and has renewed interest in this class of material. While many properties of bulk metallic glasses are still under active investigation, it has been confirmed that metallic glasses have a unique combination of various properties and are suitable for many applications, ranging from sporting equipment (Onugi et al., 1999) to MEMS (Maekawa et al., 2000).

Mechanical properties of metallic glasses have been studied for many years. Based on flow data for Pd-based metallic glasses from creep tests, uniaxial compression tests, and tensile tests, Spaepen (1977) has established an empirical deformation map. In the range in which the material can be considered a solid, two basic modes of deformation can be distinguished: homogeneous flow and inhomogeneous flow. Homogeneous flow occurs at low stresses and high temperatures as in creep tests (Chen and Goldstein, 1972). Under uniaxial tension, a specimen thins down uniformly during deformation. Inhomogeneous flow occurs at high stresses and low temperatures, where the strain localizes in a few very thin shear bands. In uniaxial tensile tests, metallic glasses exhibit very high yield strength compared to crystalline metals, but fracture occurs along a single band with little global plasticity (Leamy et al., 1972). Meanwhile, fracture toughness values ranging from 16 to 55 $\mathrm{MPa}\sqrt{\mathrm{m}}$ have been measured using compact tension and single edge notched bend geometries (Conner et al., 1997; Gilbert et al., 1997; Lowhaphandu and Lewandowski, 1998). Even higher values of fracture toughness of a Zr–Ti–Ni–Cu–Be bulk metallic glass have been measured by using a single edge notched tension geometry (Flores and Dauskardt, 1999). The high fracture toughness of metallic glasses is associated with significant plastic deformation and blunting formed by multiple shear bands and branched cracks. Multiple shear bands have also been observed in specimens loaded under other constrained geometries, such as uniaxial compression and bending (Pampillo, 1975; Hufnagel et al., 2000; Wright et al., 2001). By bonding a layer of metallic glass between two ductile metal layers, Leng and Courtney (1991) observed a high density of shear bands "trapped" between the ductile layers under tensile loading (tensile axis parallel to the layers). Recent study of a new class of ductile metal reinforced metallic glass matrix composites shows that organized shear band patterns develop throughout the sample under bending, compression, and tensile tests (Hays et al., 2000).

Some theoretical models have been put forth to explain various features of the inhomogeneous deformation in metallic glasses. Argon (1979) has shown that flow can localize in a band in which the strain rate has been perturbed, when the threshold stress for driving the local shear transformations is altered through creation of free volume. Steif et al. (1982) assumed an initial band of slightly weaker material in their analysis of strain localization and shear band. However, the origin of such a band was not considered in detail. More recently, Vaks (1991) proposed a possible mechanism for the formation of shear bands in amorphous alloys at the stage preceding the macroscopic flow.

To enable theoretical analysis for both the initial shear band formation and the post shear banding deformation, we provide a general framework within the context of continuum mechanics in the present study. In addition to the deviatoric plastic flow, we introduce an inelastic dilatational strain associated with the excess free volume as

another internal variable. Three processes compete to change the local free volume concentration and they are diffusion, annihilation, and stress-driven creation. As an example, a simple shear problem is studied in detail. Both homogeneous and inhomogeneous solutions are obtained. A linear stability analysis is performed on the basis of the homogeneous solution. Numerical simulations of the inhomogeneous solution show the development of localized shear deformation.

The plan of the paper is as follows. Section 2 describes the general formulation of the framework. In Sections 3 and 4, explicit formulae for the plastic flow and free volume generation are introduced based on a specific microscopic model. In Section 5, we consider the simple shear problem and discuss the homogeneous solution, linear stability analysis, and the inhomogeneous solution, respectively, in three subsections. Finally, some concluding remarks are given in Section 6.

## 2. General formulation

In the absence of body forces, momentum balance requires that

$$\sigma_{ij,j} = \rho \frac{\partial^2 u_i}{\partial t^2}, \tag{1}$$

where the summation convention is used for $i$, $j = 1, 2, 3$, and $()_{,j}$ denotes differentiation with respect to the $j$th spatial coordinate. $\sigma_{ij}$ are the components of the Cauchy stress tensor, $u_i$ are the components of displacement, and $\rho$ is the mass density.

Confining to the small deformation assumptions, the strain relates to the displacement gradients by

$$\varepsilon_{ij} = \tfrac{1}{2}(u_{i,j} + u_{j,i}). \tag{2}$$

However, because the strain can be extremely large inside shear bands during inhomogeneous deformation of metallic glasses, a more precise formulation should allow large strain. Nevertheless, Eq. (2) is used in this preliminary work.

In the present model of metallic glasses, the total strain consists of three parts: the elastic strain $\varepsilon^{\mathrm{e}}_{ij}$, the deviatoric plastic strain $\varepsilon^{\mathrm{p}}_{ij}$, and the inelastic dilatational strain associated with excess free volume, i.e.,

$$\varepsilon_{ij} = \varepsilon^{\mathrm{e}}_{ij} + \varepsilon^{\mathrm{p}}_{ij} + \tfrac{1}{3}(\xi - \xi_0)\delta_{ij}, \tag{3}$$

where $\xi$ is the local concentration of free volume (to be defined shortly) and $\xi_0$ is the free volume concentration at the reference state with zero strain.

We assume the metallic glasses to be isotropic and specify the constitutive laws using the invariants of the stress tensor, such as the mean stress and the Mises effective shear stress. Dividing the stress tensor into the mean stress

$$\sigma_{\mathrm{m}} = \tfrac{1}{3}(\sigma_{11} + \sigma_{22} + \sigma_{33}) \tag{4}$$

and the deviatoric stress tensor

$$s_{ij} = \sigma_{ij} - \sigma_{\mathrm{m}}\delta_{ij}. \tag{5}$$

The Mises effective shear stress is

$$\tau_e = \sqrt{\tfrac{1}{2} s_{ij} s_{ij}}. \tag{6}$$

Next, we specify the constitutive laws for the elastic strain, the deviatoric plastic strain, and the inelastic dilatational strain in turn.

The elastic strain relates to the stress by Hooke's law. For isotropic materials, we have

$$\sigma_{ij} = 2\mu \left( \varepsilon^e_{ij} + \frac{v}{1-2v} \varepsilon^e_{kk} \delta_{ij} \right), \tag{7}$$

where $\mu$ is the shear modulus and $v$ is Poisson's ratio.

The flow of the deviatoric plastic strain, $\varepsilon^p_{ij}$, is taken to be in the same direction as the deviatoric stress tensor $s_{ij}$, with the flow rate depending on the concentration of free volume $\xi$, the effective shear stress $\tau_e$, and the mean stress $\sigma_m$, namely,

$$\frac{\partial \varepsilon^p_{ij}}{\partial t} = f(\xi, \tau_e, \sigma_m) \frac{s_{ij}}{2\tau_e}. \tag{8}$$

The function $f$ can be fit to pure shear or uniaxial tensile tests.

The inelastic dilatational strain is associated with the change of the local excess free volume. The excess free volume in metallic glasses is defined as follows. Let $V$ be the volume of a sample and $V_d$ be the volume of the same sample with a dense random packaging of atoms. The excess free volume, $V_f$, is the difference between the two volumes, i.e., $V_f = V - V_d$. Define the concentration of free volume as

$$\xi = \frac{V_f}{V_d}. \tag{9}$$

In this paper, we take $\xi$ as the order parameter that describes the state of amorphous metals. To be specific, the free volume concentration is a continuum field, which can be non-uniform and can evolve with time.

There are three processes that can change the local free volume concentration: diffusion, annihilation, and generation. The diffusion of free volume is analogous to the diffusion of vacancies in crystalline materials. The free volume is redistributed by diffusion until it is spatially uniform. In crystalline materials, vacancies can annihilate at certain locations, such as grain boundaries and dislocations, where the structural requirement of crystalline translational symmetry is relaxed. In metallic glasses, this requirement does not exist and free volume can annihilate at any position simply by the atomic rearrangement. The annihilation of free volume decreases the total free volume and the metallic glasses become denser after annihilation. The generation of free volume is induced by stresses. Extra free volume can be created by a shear stress squeezing an atom into a hole smaller than itself (Spaepen, 1977). The combined rate of annihilation and generation of free volume, $g$, is taken to be a function of the local concentration of free volume $\xi$, the effective shear stress $\tau_e$, and the mean stress $\sigma_m$. Therefore, the change of free volume concentration is governed by a diffusion–production equation:

$$\frac{\partial \xi}{\partial t} = D\xi_{,ii} + g(\xi, \tau_e, \sigma_m), \tag{10}$$

where the diffusivity $D$ is a function of temperature, but is taken to be independent of the free volume concentration and the stresses.

Eqs. (1)–(10) provide a general framework for inhomogeneous deformation in metallic glasses. The specific functions for the plastic flow, $f(\xi, \tau_e, \sigma_m)$, and the production rate of free volume, $g(\xi, \tau_e, \sigma_m)$, are discussed in the following two sections. Note that the functions are based on a specific microscopic model. As theories and experiments are refined, more appropriate functions may emerge. We will proceed within the general framework using the existing functions and leave detailed modifications to subsequent work.

## 3. Flow equation

Based on the free volume theory Cohen and Turnbull (1959); Turnbull and Cohen, 1961, 1970; Spaepen (1977) derived a flow equation for metallic glasses under a shear stress $\tau$:

$$\frac{\partial \gamma^p}{\partial t} = 2v_0 \exp\left[-\frac{\alpha v^*}{v_f} - \frac{\Delta G^m}{k_B T}\right] \sinh\left[\frac{\tau \Omega}{2k_B T}\right], \tag{11}$$

where $\gamma^p$ is the plastic shear strain, $v_f$ the average free volume per atom, $v^*$ a critical volume (the effective hard-sphere volume of an atom, for example), $\alpha$ a geometrical factor of order unity, $v_0$ the frequency of atomic vibration, $\Delta G^m$ the activation energy, $\Omega$ the atomic volume, $k_B$ the Boltzmann's constant, and $T$ the absolute temperature.

According to Eq. (11), the plastic strain rate increases as the applied shear stress increases. At a low stress, $\sinh\left[\frac{\tau\Omega}{2k_BT}\right] \approx \frac{\tau\Omega}{2k_BT}$, and Eq. (11) recovers the linear Newtonian viscous behavior. Furthermore, the flow rate depends on the average free volume per atom. At a constant stress, the strain rate is higher when the average free volume is larger. Changing the free volume can radically change the flow rate. Steif et al. (1982) showed that the softening induced by increasing the free volume permits localized deformation.

For multiaxial stress states, we replace the shear stress $\tau$ in Eq. (11) with the Mises effective shear stress $\tau_e$. The concentration of free volume defined in Eq. (9) can be approximately taken as $\xi = v_f/v^*$. Thus, from Eq. (11), we obtain a formula for the function $f$ in the general flow Eq. (8) as below

$$f(\xi, \tau_e) = 2R \exp\left[-\frac{\alpha}{\xi}\right] \sinh\left[\frac{\tau_e \Omega}{2k_B T}\right], \tag{12}$$

where $R = v_0 \exp\left[-\frac{\Delta G^m}{k_B T}\right]$ and $1/R$ defines a time. Using the typical values of $v_0$ ($\sim 10^{13}$ $s^{-1}$), $\Delta G^m$ ($\sim 10^{-19}$ J), and $k_B T$ ($\sim 5 \times 10^{-21}$ J, corresponding to $T \sim 400$ K), we have $R \sim 2 \times 10^4$ $s^{-1}$.

Note that the flow rate function in Eq. (12) is independent of the mean stress, $\sigma_m$. Although the earlier work conducted on thin ribbons of amorphous Pd–Cu–Si reported a slight pressure dependence of the flow/fracture behavior, it was noted that there may have been problems with alignment and gripping which facilitated deformation

and fracture at the grip ends (Davis and Kavesh, 1975). The recent study on the flow and fracture behavior of a Zr–Ti–Ni–Cu–Be bulk metallic glass showed that the flow stress and fracture strain are essentially independent of superimposed hydrostatic pressure over the range from 50 to 575 MPa (Lowhaphandu et al., 1999). However, the pressure is low compared to the yield stress of metallic glasses (1–2 GPa) and one might reasonably expect that the effect could only become important at higher pressures. Flores and Dauskardt (2001) showed in their experiments a critical tensile mean stress of 0.95 GPa and proposed a strain localization model with the effect of mean stress. While the mean stress effect on the flow behavior of metallic glasses is still under investigation, in the present study we include the effect in the flow equation for the general scheme (Eq. (8)), but set it to be zero in the example problem.

## 4. Free volume creation and annihilation

The concentration of free volume plays the role as an order parameter in the present framework. An as-prepared metallic glass is thermodynamically unstable and has a non-equilibrium amount of free volume. The free volume is continuously being annihilated by structural relaxation toward the metastable equilibrium configuration (Taub and Spaepen, 1980). Meanwhile, applying stresses can create free volume. In the model by Spaepen (1977), free volume is created by an applied shear stress $\tau$ and annihilated by a series of atomic jumps, and the net rate of the change of free volume is

$$\frac{\partial v_{\mathrm{f}}}{\partial t} = v^* v_0 \exp\left[-\frac{\Delta G^{\mathrm{m}}}{k_{\mathrm{B}}T} - \frac{\alpha v^*}{v_{\mathrm{f}}}\right]\left\{\frac{2\alpha k_{\mathrm{B}}T}{S v_{\mathrm{f}}}\left(\cosh\frac{\tau\Omega}{2k_{\mathrm{B}}T} - 1\right) - \frac{1}{n_D}\right\}, \tag{13}$$

where $n_D$ is the number of atomic jumps needed to annihilate a free volume equal to $v^*$, and $S = \frac{2}{3}\frac{1+v}{1-v}\mu$.

From Eq. (13), we obtain a formula for the function $g$ in Eq. (10), again by taking $\xi = v_{\mathrm{f}}/v^*$ and replacing $\tau$ with $\tau_{\mathrm{e}}$, namely

$$g(\xi, \tau_{\mathrm{e}}) = R\exp\left[-\frac{\alpha}{\xi}\right]\left\{\frac{\alpha}{\beta\bar{\mu}\xi}\left(\cosh\frac{\tau_{\mathrm{e}}\Omega}{2k_{\mathrm{B}}T} - 1\right) - \frac{1}{n_D}\right\}, \tag{14}$$

where

$$\beta = \frac{2}{3}\frac{1+v}{1-v}\frac{v^*}{\Omega}, \quad \bar{\mu} = \frac{\mu\Omega}{2k_{\mathrm{B}}T}. \tag{15}$$

Notice that the effect of mean stress on the creation and annihilation of free volume has not been taken into account in Eq. (14). Equations modeling the effect of mean stress on free volume have been proposed by other studies (Steif, 1983; Flores and Dauskardt, 2001). Here, we include the effect in the general scheme (Eq. (10)), but neglect it in the following analysis.

Fig. 1 schematically shows the rate function, Eq. (14), versus the free volume concentration for constant effective shear stresses. When $\tau_{\mathrm{e}} = 0$, there is no stress-driven creation of free volume and the concentration of free volume decreases as the result

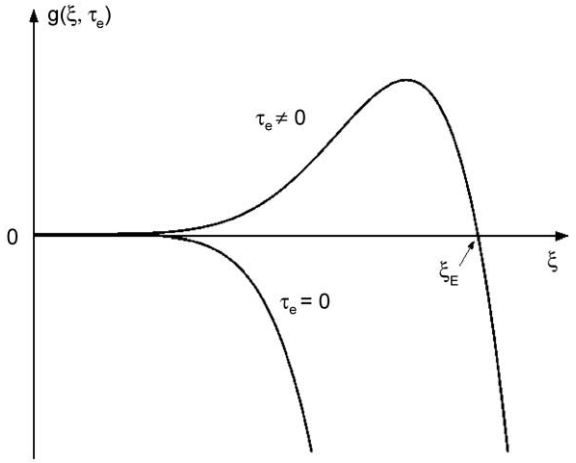


Fig. 1. The combined rate function of annihilation and stress-driven creation of free volume from Spaepen's microscopic model.

of free volume annihilation. The rate is very small as the free volume concentration approaches zero, but the process does not stop until the free volume concentration is zero. However, since certain amount of free volume should exist in the metastable equilibrium configuration to allow plastic flow, a better formula would have a non-zero equilibrium value of the free volume concentration. When $\tau_e \neq 0$, there exists a steady state, at which the stress-driven creation and the annihilation are balanced. The steady state value of the free volume concentration, $\xi_E$, increases as the effective shear stress increases.

A comparison of the production rate in Eq. (14) with the diffusion term in the right-hand side of Eq. (10) defines a length:

$$l = \sqrt{\frac{D}{R}}. \tag{16}$$

Thus, the diffusivity $D$ takes the form

$$D = v_0 \exp\left[-\frac{\Delta G^m}{k_B T}\right] l^2. \tag{17}$$

Eq. (17) has the same form as the diffusivity for vacancies in crystalline materials, where the length scale is comparable to the diameter of atoms. Assuming the similar mechanism for the diffusion of free volume, we estimate $l \sim 0.1$ nm. However, the mechanisms of free volume diffusion in metallic glasses are not well understood; in particular, it is not clear that the free volume diffuses by a vacancy-like mechanism.

## 5. Example: simple shear problem

Consider a layer of width $2h$ ($h \gg l$) in the $x$ direction, as shown in Fig. 2. The dimensions of the layer in the $y$ and $z$ directions are much larger than $h$ and are

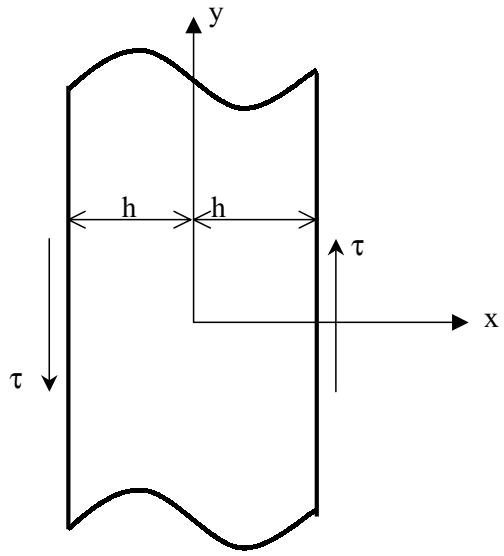


Fig. 2. Geometric configuration of a simple shear problem.

assumed to be infinity. The layer is loaded with a constant average shear strain rate. The strain rate is assumed to be low, falling in the quasi-static range, such that we can neglect the inertial term in the momentum equation, Eq. (1).

Under the quasi-static assumption, the force equilibrium requires that the shear stress be spatially uniform but time-dependent, i.e., $\tau = \tau(t)$. As the shear stress creates more free volume, the sample dilates. When the dilation is non-uniform across the layer, geometric constraint will induce normal stresses in the $y$ and $z$ directions. The stresses are assumed equal in both directions, i.e., $\sigma_{yy} = \sigma_{zz} = \sigma(x,t)$, and the total stress after integrating across the layer is zero

$$\int_{-h}^{h} \sigma(x,t)\,\mathrm{d}x = 0. \tag{18}$$

In the $x$ direction, the material dilates freely with no constraint and the normal stress is zero. Under such a stress state, the effective shear stress is

$$\tau_{\mathrm{e}} = \sqrt{\tau^2 + \tfrac{1}{3}\sigma^2}. \tag{19}$$

The total shear strain, $\gamma$, consists of the elastic strain, $\gamma^{\mathrm{e}}$, and the plastic strain, $\gamma^{\mathrm{p}}$. The elastic shear strain relates to the shear stress by Hooke's law, and the plastic strain flows according to Eq. (8). Thus, the total shear strain rate is

$$\frac{\partial \gamma}{\partial t} = \frac{1}{\mu}\frac{\mathrm{d}\tau}{\mathrm{d}t} + f(\xi, \tau_{\mathrm{e}})\frac{\tau}{\tau_{\mathrm{e}}}. \tag{20}$$

The average shear strain rate is

$$r = \frac{1}{2h}\int_{-h}^{h} \frac{\partial \gamma}{\partial t}\,\mathrm{d}x. \tag{21}$$

Integration of both the sides of Eq. (20) with respect to $x$ from $-h$ to $h$ leads to

$$\frac{\mathrm{d}\tau}{\mathrm{d}t} = \mu\left[r - \frac{1}{2h}\int_{-h}^{h} f(\xi,\tau_e)\frac{\tau}{\tau_e}\,\mathrm{d}x\right]. \tag{22}$$

We assume that, by the geometric constraint, the normal strains are equal in the $y$ and $z$ directions and they are spatially uniform, i.e., $\varepsilon_{yy} = \varepsilon_{zz} = \varepsilon(t)$. The normal strain consists of the elastic strain, the plastic strain, and the dilatational strain associated with free volume. The total normal strain rate is

$$\frac{\mathrm{d}\varepsilon}{\mathrm{d}t} = \frac{1-2\nu}{2\mu}\frac{\partial \sigma}{\partial t} + f(\xi,\tau_e)\frac{\sigma}{6\tau_e} + \frac{1}{3}\frac{\partial \xi}{\partial t}. \tag{23}$$

By integrating both the sides of Eq. (23) with respect to $x$ from $-h$ to $h$ and applying Eq. (18) for the first term at the right-hand side, we obtain

$$\frac{\mathrm{d}\varepsilon}{\mathrm{d}t} = \frac{1}{2h}\int_{-h}^{h}\left[f(\xi,\tau_e)\frac{\sigma}{6\tau_e} + \frac{1}{3}\frac{\partial \xi}{\partial t}\right]\mathrm{d}x. \tag{24}$$

Assuming that the concentration of free volume is uniform along the $y$ and $z$ directions but varies along the $x$ direction, Eq. (10) becomes

$$\frac{\partial \xi}{\partial t} = D\frac{\partial^2 \xi}{\partial x^2} + g(\xi,\tau_e). \tag{25}$$

Eqs. (22)–(25) are coupled together and have to be solved simultaneously for the shear stress, the normal strain, the normal stress, and the free volume concentration. The shear strain can be computed from Eq. (20) after solving the coupled equations.

### 5.1. Homogeneous deformation

If the initial distribution of the free volume is uniform across the layer, there exists a set of homogeneous solutions to Eqs. (22)–(25) and the deformation is homogeneous, i.e.,

$$\gamma_h = rt, \tag{26a}$$

$$\sigma_h = 0, \tag{26b}$$

$$\frac{\mathrm{d}\tau_h}{\mathrm{d}t} = \mu[r - f(\xi_h,\tau_h)], \tag{26c}$$

$$\frac{\mathrm{d}\varepsilon_h}{\mathrm{d}t} = \tfrac{1}{3}g(\xi_h,\tau_h), \tag{26d}$$

$$\frac{\mathrm{d}\xi_h}{\mathrm{d}t} = g(\xi_h,\tau_h). \tag{26e}$$

The shear strain in the above homogeneous solution is uniformly distributed, increasing linearly with time at the prescribed constant strain rate. Since the deformation is homogeneous, the normal stress due to the geometric constrain is zero and the normal strain is purely dilatational. The variations of the shear stress and the free volume concentration with time are obtained by numerically integrating Eqs. (26c) and (26e) for the given strain rate, $r$. The solution is similar to that obtained by Steif et al. (1982) except for the normal strain in Eq. (26d).

Fig. 3a shows the stress–strain curve of the homogeneous deformation and Fig. 3b shows the concentration of free volume versus the shear strain for normalized strain rate $r/R = 10^{-6}$. The initial concentration of free volume is taken to be 0.008 and the initial stress is zero. The material parameters used in the calculations are: $\bar{\mu} = 120$, $\alpha = 0.15$, $\beta = 1$, $n_D = 3$. The shear stress drops after an initial elastic response and the free volume concentration increases concurrently, indicating a homogeneous softening of the material. The homogeneous deformation eventually reaches a steady state, at which both the free volume concentration and the shear stress are constant and the metallic glass flows like a liquid. The steady state values of the shear stress and free volume concentration correspond to the steady state point in Fig. 1 and depend on the prescribed strain rate.

### 5.2. Linear stability analysis

The stability of the homogeneous deformation may be investigated by seeking an inhomogeneous solution with small perturbations from the homogeneous solution

$$\xi = \xi_h + \delta_\xi(t)\sin(kx), \tag{27a}$$

$$\gamma = \gamma_h + \delta_\gamma(t)\sin(kx), \tag{27b}$$

$$\sigma = \sigma_h + \delta_\sigma(t)\sin(kx), \tag{27c}$$

where $k$ is the wave number of the perturbations, and $(\delta_\xi,\ \delta_\gamma,\ \delta_\sigma)$ denote the amplitudes of the perturbations, assumed to be small compared to $(\xi_h,\ \gamma_h,\ \tau_h)$. The shear stress $\tau$ and the dilatational strain $\varepsilon$ are required to be homogeneous and have no perturbations. This method is commonly used when the homogeneous solution is time-independent; however, it has been employed in time-dependent cases by Clifton (1980), Bai (1982), and Fressengeas and Molinari (1987) for thermo-plastic instability analysis. In those cases, it is assumed that the growth rate of the perturbation is much greater than the rate of the homogeneous solution.

Substitutions of Eq. (27) into Eqs. (25), (20), and (23), and retaining only the first order terms of $\delta_\xi$, $\delta_\gamma$, and $\delta_\sigma$ lead to

$$\frac{\mathrm{d}\delta_\xi}{\mathrm{d}t} = \left[\frac{\partial g}{\partial \xi} - k^2 l^2\right]\delta_\xi, \tag{28a}$$

$$\frac{\mathrm{d}\delta_\gamma}{\mathrm{d}t} = \frac{\partial f}{\partial \xi}\delta_\xi, \tag{28b}$$

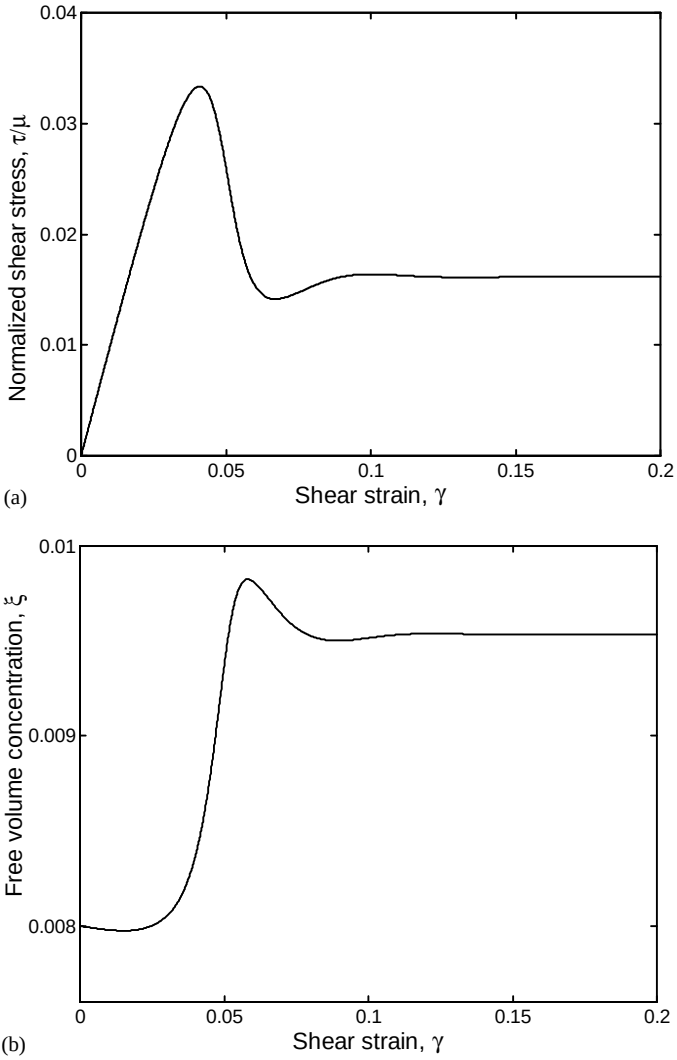


Fig. 3. Results from the homogeneous solution of the simple shear problem with normalized strain rate $r/R = 10^{-6}$: (a) shear stress versus shear strain; (b) free volume concentration versus shear strain.

$$\frac{\mathrm{d}\delta_\sigma}{\mathrm{d}t} = -\frac{f(\xi_h, \tau_h)}{6\tau_h}\delta_\sigma - \frac{1}{3}\left[\frac{\partial g}{\partial \xi} - k^2 l^2\right]\delta_\xi, \tag{28c}$$

where $\partial g/\partial \xi$ and $\partial f/\partial \xi$ are evaluated at the homogeneous solution, $(\xi_h, \tau_h)$. The time $t$ in Eq. (28) has been scaled by $1/R$ and the rate functions, $f$ and $g$, have been scaled accordingly by $R$.

From Eq. (28a), the perturbation to the concentration of free volume will amplify if $(\partial g/\partial \xi) > k^2 l^2$. From Eq. (28b), the perturbation to the shear strain will amplify

as the perturbation to the concentration of free volume amplifies. From Eq. (28c), the growth of the perturbation to the free volume concentration induces the growth of compressive normal stress, but the amplitude of the stress decreases as the result of relaxation through plastic flow.

From the above analysis, we see that the stability of the homogeneous solution depends on the perturbation to the free volume concentration, which is governed by three processes: diffusion, annihilation, and creation. The diffusion of free volume is slow for small wave number perturbations (i.e., long wavelengths) and fast for large wave number perturbations (i.e., short wavelengths). The annihilation of free volume mostly depends on temperature, slow at low temperature and fast at high temperature. The stress-driven creation of free volume is slow at low stresses and fast at high stresses. The diffusion and annihilation processes cause the perturbation to decay, and the creation process causes the perturbation to amplify. The stability of the homogeneous deformation is determined by the competition of these three processes.

As seen in Eq. (26) and Fig. 3, both the shear stress and the free volume concentration in the homogeneous deformation are changing over the time. Once the combination of the shear stress and free volume satisfies the condition, $(\partial g/\partial \xi) > k^2 l^2$, the homogeneous deformation becomes unstable and the perturbations start to grow. Fig. 4 shows the variation of $\partial g/\partial \xi$ (scaled by $R$) from the homogeneous solution for the normalized strain rate $r/R = 10^{-6}$. The maximum value of $(\partial g/\partial \xi)$ defines a critical wave number satisfying $k_c^2 l^2 = \max[\partial g/\partial \xi]$. The homogeneous deformation is stable for $k > k_c$ and unstable for $k < k_c$. The critical wave number depends on the prescribed strain rate, as shown in Fig. 5.

Note that the linear perturbation analysis is only valid for a short time after instability and cannot predict the whole process of inhomogeneous deformation. Eqs. (22)–(25) must be solved numerically for the complete solution of inhomogeneous deformation.

### 5.3. Inhomogeneous deformation

The deformation of the metallic glass layer will be inhomogeneous if the initial free volume is not uniformly distributed. In practice, the non-uniform distribution of free volume may be the result of quenching processes or due to thermal fluctuation. Assume a finite amplitude disturbance in the form of a Gauss function is added to the initial distribution of free volume, i.e.,

$$\xi(x,0) = \xi_i + \delta \exp\left[-\frac{(x-x_0)^2}{\Delta^2}\right], \tag{29}$$

where $\xi_i$ is a constant, $\delta$ is the amplitude of the disturbance, $x_0$ is the location, and $\Delta$ is the characteristic half width. It is assumed that $\Delta \ll h$ such that the boundaries of the layer at $x = \pm h$ are far away from the disturbance and therefore, have little effect on the evolution of the disturbance. In the following numerical simulation, we take $\xi_i = 0.008$, $\delta = 0.001$, $x_0 = 0$, $\Delta = 100l$, and $h = 2000l$. The stresses and strains are assumed to be zero in the initial configuration.

Eq. (25) is solved by the finite element method and a semi-implicit algorithm is used for the time integration. The integrations with respect to $x$ in Eqs. (22) and (24) are

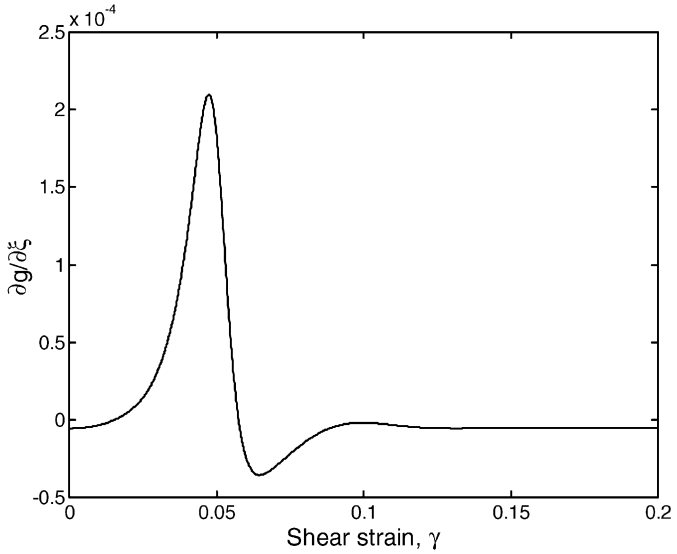


Fig. 4. Variation of $\partial g/\partial \xi$ (scaled by $R$) from the homogeneous solution of the simple shear problem.

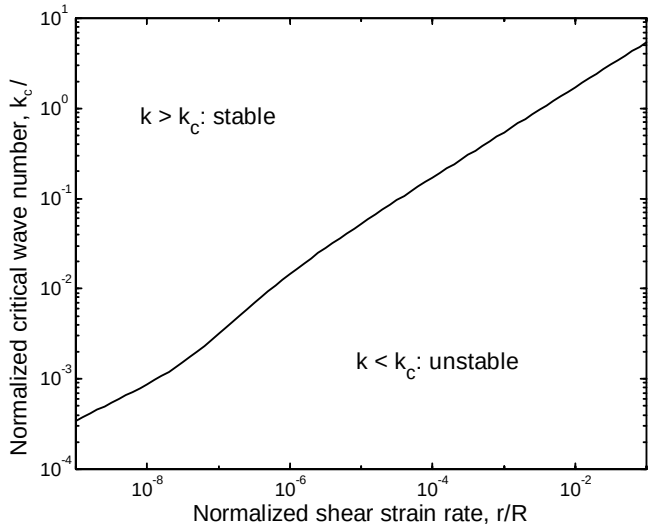


Fig. 5. Stability analysis of the homogeneous deformation: critical wave number versus shear strain rate.

computed by the Gaussian quadrature. Since the boundary of the layer is far away from the disturbance ($h \gg \Delta$), the free volume is uniformly distributed near the boundaries and $\partial \xi/\partial x = 0$ is assumed at the boundaries. At each time step, the shear stress and the free volume concentration at the next time step are computed from Eqs. (22) and (25), respectively, using the values at the current time step; then, the normal strain is

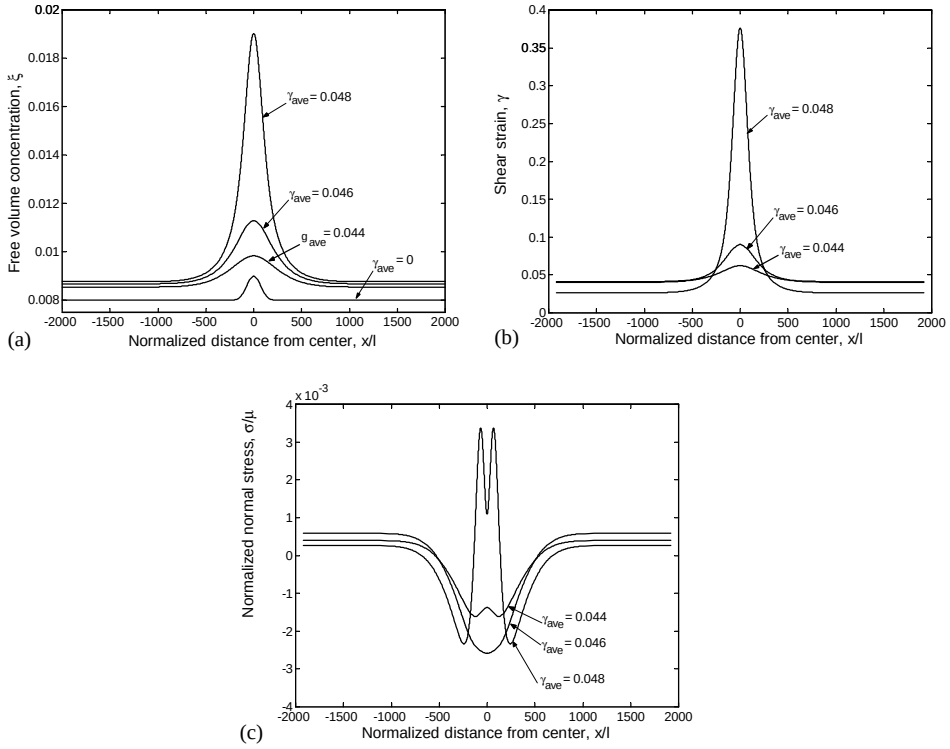


Fig. 6. Results from the numerical simulation of the inhomogeneous deformation: distributions of (a) free volume concentration, (b) shear strain and (c) normal stress.

computed from Eq. (24), after which the normal stress is computed at each integration point from Eq. (23); the shear strains at the integration points are computed from Eq. (20) although it is not necessary for the computations at the next time step.

Figs. 6 and 7 show the results of a numerical simulation of the inhomogeneous deformation with the prescribed average shear strain rate $r = 10^{-6}R$. Fig. 6a shows the distributions of the free volume at different time steps, where the time is indicated by the average shear strain, $\gamma_{\text{ave}} = rt$. Figs. 6b and c show the distributions of the shear strain and the normal constraining stress. Fig. 7 shows the shear stress versus the average shear strain. At the initial stage of the deformation, the stress is low and the change of the free volume is dominated by the diffusion and annihilation processes. At this stage, the amplitude of the initial disturbance to the free volume concentration decays, the deformation is nearly homogeneous and elastic. As the shear stress increases, the creation process of the free volume becomes more significant. The amplitude of the disturbance starts to grow at $\gamma_{\text{ave}} \approx 0.04$, when the creation process starts to dominate the diffusion and annihilation. As shown in Fig. 6a, the free volume concentration at the center of the disturbance grows much faster than it does elsewhere. Meanwhile, the shear strain grows rapidly at the center, but increases

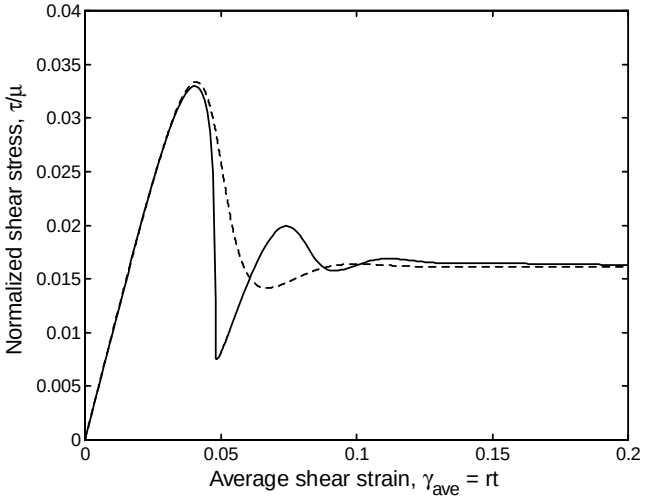


Fig. 7. Variation of the shear stress from the numerical simulation of the inhomogeneous deformation with $r/R = 10^{-6}$. The dashed line is from the corresponding homogeneous solution.

slowly and even decreases at the other location, which develops a localized distribution of the shear deformation, as shown in Fig. 6b. The inhomogeneous growth of the free volume causes inhomogeneous dilatation of the material, which in turn causes the constraining normal stress, as shown in Fig. 6c. The normal stress is relatively small comparing to the shear stress. As the free volume and shear strain start to localize, the shear stress drops abruptly from a maximum stress, as shown in Fig. 7. As the shear stress drops to a lower level, the diffusion and annihilation processes regain the dominance against the creation process and eventually stop the localization process. Similar behaviors have been observed in the uniaxial compression tests, where shear bands formed, propagated, and then stop (Wright et al., 2001). Finally, the deformation approaches the homogeneous steady state and the distribution of free volume becomes uniform.

The results of the numerical simulation are sensitive to several parameters. For instance, very different behavior can be obtained if a different value of $\alpha$ in Eqs. (12) and (14) is used, or if a different value of the initial free volume concentration ($\xi_i$) is used. In some cases, the localization of free volume is so severe that the shear stress drops to zero before the localization stops, a different behavior as observed in the uniaxial tensile tests.

## 6. Concluding remarks

A framework for inhomogeneous deformation in metallic glasses has been presented. The free volume concentration is adopted as the order parameter of the amorphous material systems. The specific rate functions for the free volume generation and plastic

flow depend on the underlying microscopic model, but the framework is generally valid for other models.

As an example, the simple shear problem is solved. Both homogeneous and inhomogeneous solutions are obtained and the results are based on the chosen rate functions, obtained from a simple extension of the microscopic model by Spaepen (1977). The numerical simulation shows the development of the inhomogeneous deformation and the strain localization.

## Acknowledgements

The work at Princeton is supported by the National Science Foundation through Grants CMS-9820713 and CMS-9988788 with Drs. Ken Chong and Jorn Larsen-Basse as the program directors. ZS thanks helpful discussions with Professors A.G. Evans, F. Spaepen, R.H. Dauskardt, and D. Srolovitz. The work at Stanford (WDN) was supported by the Air Force Office of Scientific Research under AFOSR Grant No. F49620-98-1-0260.

## References

Argon, A.S., 1979. Plastic deformation in metallic glasses. Acta Metall. 27, 47–58.

Bai, Y.L., 1982. Thermo-plastic instability in simple shear. J. Mech. Phys. Solids 30 (4), 195–207.

Chen, H.S., Goldstein, M., 1972. Anomalous viscoelastic behavior of metallic glasses of Pd–Si-Based alloys. J. Appl. Phys. 43 (4), 1642.

Clifton, R.J., 1980. Material response to ultra-high loading rates. NRC Report No. 356, US National Material Advisory Board.

Cohen, M.H., Turnbull, D., 1959. Molecular transport in liquids and glasses. J. Chem. Phys. 31 (5), 1164–1169.

Conner, R.D., Rosakis, A.J., Johnson, W.L., Owen, D.M., 1997. Fracture toughness determination for a beryllium-bearing bulk metallic glass. Scr. Mater. 37 (9), 1373–1378.

Davis, L.A., Kavesh, S., 1975. J. Mater. Sci. 10, 453.

Flores, K.M., Dauskardt, R.H., 1999. Enhanced toughness due to stable crack tip damage zones in bulk metallic glass. Scr. Mater. 41 (9), 937–943.

Flores, K.M., Dauskardt, R.H., 2001. Mean stress effects on flow localization and failure in a bulk metallic glass. Acta Mater. 49 (13), 2527–2537.

Fressengeas, C., Molinari, A., 1987. Instability and localization of plastic flow in shear at high strain rates. J. Mech. Phys. Solids 35 (2), 185–211.

Gilbert, C.J., Ritchie, R.O., Johnson, W.L., 1997. Fracture toughness and fatigue-crack propagation in a Zr–Ti–Ni–Cu–Be bulk metallic glass. Appl. Phys. Lett. 71 (4), 476–478.

Hays, C.C., Kim, C.P., Johnson, W.L., 2000. Microstructure controlled shear band pattern formation and enhanced plasticity of bulk metallic glasses containing in situ formed ductile phase dendrite dispersions. Phys. Rev. Lett. 84 (13), 2901–2904.

Hufnagel, T.C., El-Deiry, P., Vinci, R.P., 2000. Development of shear band structure during deformation of a $Zr_{57}Ti_5Cu_{20}Ni_8Al_{10}$ bulk metallic glass. Scr. Mater. 43 (12), 1071–1075.

Johnson, W.L., 1999. Bulk glass-forming metallic alloys: science and technology. MRS Bull. 24 (10), 42–56.

Klement, W., Willens, R.H., Duwez, P., 1960. Nature 187, 869.

Leamy, H.J., Chen, H.S., Wang, T.T., 1972. Plastic flow and fracture of metallic glass. Metall. Trans. 3, 699–708.

Leng, Y., Courtney, T.H., 1991. Multiple shear band formation in metallic glasses in composites. J. Mater. Sci. 26, 588–592.

Lowhaphandu, P., Lewandowski, J.J., 1998. Fracture toughness and notched toughness of bulk amorphous alloy: Zr–Ti–Ni–Cu–Be. Scr. Mater. 38 (12), 1811–1817.

Lowhaphandu, P., Montgomery, S.L., Lewandowski, J.J., 1999. Effects of superimposed hydrostatic pressure on flow and fracture of a Zr–Ti–Ni–Cu–Be bulk amorphous alloy. Scr. Mater. 41 (1), 19–24.

Maekawa, S., Takashima, K., Shimojo, M., Higo, Y., Swain, M.V., 2000. Fatigue properties for micro-sized Ni–P amorphous alloy specimens. Mat. Res. Soc. Symp. Proc. 605, 247–252.

Onugi, M., Inoue, A., Yamaguchi, T., Minamiguchi, H., Iwata, K., 1999. Mater. Jpn. 38, 251.

Pampillo, C.A., 1975. Flow and fracture in amorphous alloys. J. Mater. Sci. 10 (7), 1194–1227.

Spaepen, F., 1977. A microscopic mechanism for steady state inhomogeneous flow in metallic glasses. Acta Metall. 25, 407–415.

Steif, P.S., Spaepen, F., Hutchinson, J.W., 1982. Strain localization in amorphous metals. Acta Metall. 30, 447–455.

Steif, P.S., 1983. Ductile versus brittle behavior of amorphous metals. J. Mech. Phys. Solids 31 (5), 359–388.

Taub, A.I., Spaepen, F., 1980. The kinetics of structural relaxation of a metallic glass. Acta Metall. 28, 1781–1788.

Turnbull, D., Cohen, M.H., 1961. Free-volume model of the amorphous phase: glass transition. J. Chem. Phys. 34 (1), 120–125.

Turnbull, D., Cohen, M.H., 1970. On the free volume model of the liquid–glass transition. J. Chem. Phys. 52 (6), 3038–3041.

Vaks, V.G., 1991. Possible mechanism for formation of localized shear bands in amorphous alloys. Phys. Lett. A 159, 174–178.

Wright, W.J., Saha, R., Nix, W.D., 2001. Deformation mechanisms of the $Zr_{40}Ti_{14}Ni_{10}Cu_{12}Be_{24}$ bulk metallic glass. Mater. Trans. JIM 42 (4), 642–649.